

Strain-Controlled RheoSANS Instrument for the Measurement of the Microstructural, Electrical and Mechanical Properties of Soft Materials

Jeffrey J. Richards¹, Norman J. Wagner², Paul D. Butler^{1,*}

¹NIST Center for Neutron Research, National Institute of Standards and Technology, Gaithersburg, MD 20899, USA

²Center for Neutron Science, Department of Chemical and Biomolecular Engineering, University of Delaware Newark, DE 98195, USA

*Corresponding Author – Paul Butler, Paul.Butler@nist.gov, P: 301-975-2028.

I. ABSTRACT.

In situ measurements are an increasingly important tool to inform the complex relationship between nanoscale properties and macroscopic material measurements. Knowledge of these phenomena can be used to develop new materials to meet the performance demands of next generation technologies. Conductive complex fluids have emerged as an area of research where the electrical and mechanical properties are key design parameters. To study the relationship between microstructure, conductivity and rheology, we have developed a small angle neutron scattering (SANS) compatible Couette rheological geometry capable of making impedance spectroscopy measurements under continuous shear. We have also mounted this geometry on a commercial strain controlled rheometer with a modified Forced Convection Oven (FCO). In this manuscript, we introduce the simultaneous measurement of impedance spectroscopy, rheological properties and SANS data. We describe the validation of this Dielectric RheoSANS instrument and demonstrate its operation using two systems - an ion gel comprised of Pluronic® surfactant and ionic liquid, ethyl-ammonium nitrate, and poly(3-hexylthiophene) organogel prepared in a mixture of hexadecane and dichlorobenzene. In both systems, we use this new measurement capability to study the microstructural state of these materials under two different protocols. By

Monitoring their dielectric rheology at the same time as the SANS measurement, we demonstrate the capacity to directly probe structure-property relationships inherent to the macroscopic material response.

II. INTRODUCTION.

In situ measurements are increasingly used to interrogate the intrinsic properties of suspensions of conducting particles, self-assembled systems, and nanocomposites.¹⁻⁵ When two measurements are combined, for example in dielectric rheology (DR), the macroscopic material response can be understood based on the complex relationships between a material's electrical and mechanical properties. The combination of small amplitude oscillatory shear (SAOS) with impedance spectroscopy (IS) for instance can be used to probe fundamental relaxation processes in materials. This has been used to study dielectric and mechanical relaxation spectra of entangled polymers that arise due to dipole-dipole correlations with global chain motion.^{6,7} DR is also particularly powerful for the study of kinetic processes where both the electrical and mechanical properties of a material evolve due to a chemical reaction or gelation process. In emerging methods, shear is applied and the microstructural rearrangement imposed by the macroscopic flow field is probed using IS.^{1,2} In this case, the dielectric response arises due to microstructural state of the material. Underlying these experiment techniques is the intrinsic link between a material's macroscopic response and its underlying microstructure. DR, however, only probes this underlying microstructural response indirectly. Indeed, it is only through development of constitutive relationships between microstructure and macroscopic measurements that the true nature of the material response can be reconstructed.

An alternative approach is to simply measure the material microstructure directly. That knowledge of the instantaneous microstructural state is often sufficient to reconstruct

Microscopic measurements has been demonstrated experimentally.⁸⁻¹⁰ Small angle neutron scattering (SANS) is ideal for this application as it provides information both about the disperse phase material's size, shape, and composition as well as information associated with colloidal interactions in suspensions.¹¹ Shear cells compatible with SANS measurements are deployed at SANS and SAXS beam-lines around the world capable of examining a sample confined within a Couette geometry along the vorticity, shear-gradient and flow directions.¹²⁻¹⁶ The progress in measurement sciences made by these shear geometries have led to the development and validation of commercially available RheoSANS instruments.^{17,18} RheoSANS increased the utility of shear cells making direct measurement of structure-stress relationships possible.^{8,19} Coupled with event mode data acquisition, where the time and position of each neutron is tracked, and using a two-way handshaking protocol, time-dependent shear experiments with resolutions approaching 10 millisecond intervals have also opened the door to a deeper understanding of both steady state and time-dependent material response.²⁰

More recently, in situ rheology measurements have been expanded to combine other techniques such as Raman spectroscopy.²¹ Also, the combination of DR, RheoSANS, and Dielectric SANS was used to study the in situ mechanical and microstructural response of a conjugated polymer organogel undergoing thermo-reversible gelation.^{22,23} These past investigations and the future goal of examining materials under increasingly complex experimental protocols has motivated the development of a Dielectric RheoSANS instrument capable of in situ SANS, electrical and stress measurements.²⁴ The technical specifications of the geometry and the modifications necessary to install it on a commercial strain-controlled rheometer are described in detail elsewhere.²⁴ In this manuscript, we validate the performance of the dielectric geometry for simultaneous SANS experiments, impedance spectroscopy, and

ological testing using both oscillatory rheology and steady shear. We show that the design of the Couette geometry provides the means to perform all tests without compromising the accuracy or precision of the SANS, dielectric or rheological information over the entire accessible shear rate range of the rheometer. We also demonstrate the application of the Dielectric RheoSANS technique using two case studies: 1.) *The self-assembly of poly(3-hexylthiophene) organogel networks*, and 2.) *Shear induced crystalline alignment of Pluronic® micelles in an ion gel*.

III. Dielectric RheoSANS Description:

III.A Dielectric RheoSANS Geometry

Advanced DR instrumentation commonly uses liquid metals to maintain electrical contact under arbitrary deformation profiles, allowing for experiments to be performed on samples in their quiescent state and far from equilibrium such as under applied shear flow. Common DR instruments also employ parallel plate geometries to simplify sample loading and impedance correction as the electrical cell constant is only a function of plate diameter and the gap spacing.^{1,2} While much about the electrical response of materials to applied shear can be learned from such instruments, there are several limitations. First, for a stress-controlled rheometer, the liquid metal contact contributes a non-negligible resistance to the measured torque. Second, the electrical response in a parallel plate geometry under steady shear represents an average over the radial shear profile and therefore, is itself a convolution of the true macroscopic material response. Finally, the construction of parallel plate geometries compatible with SANS measurements has proven challenging. Consequently, the Couette geometry is preferred for the Dielectric RheoSANS technique.

Genz et al. demonstrated a Couette geometry compatible with rheo-impedance measurements of carbon black suspensions in mineral oil.²⁵ In their custom-built instrument, the shear rate is

constant across the entire gap and they probed the electrical properties of the material along the shear gradient projection of the deformation. This instrument represents an important improvement as compared with parallel plate geometries for the measurement of the electrical and rheological response of a material under steady shear. A further improvement can be made using a strain-controlled rheometer with an independent torque transducer. This effectively decouples the application of strain from the measurement of torque so there is no torque correction necessary. Therefore, our design begins with a Couette Geometry attached to a strain-controlled rheometer. The radial cross-section is shown in Figure 1. In this geometry, the sample is confined between two cylinders ($d_{o,bob}=25.1$ mm and $d_{i,cup}=27$ mm) that are mounted to an ARES G2 Rheometer (TA Instruments – Newark, DE).²⁶ The inner bob cylinder is 34 mm tall and capped on the bottom with a 4° cone angle truncated to operate at a 100-micron gap. The cup and bob walls are machined from titanium and are 0.5 mm thick in the hollow region to balance neutron transparency with mechanical integrity.¹⁸ The cap, the bottom of the cup, and the bob shaft are machined from Poly(ether ether ketone) (PEEK) to electrically isolate the impedance measurement from the instrument and to reduce fringing. They are bonded to the titanium walls with a high-temperature two-part epoxy (3M DP420).²⁴

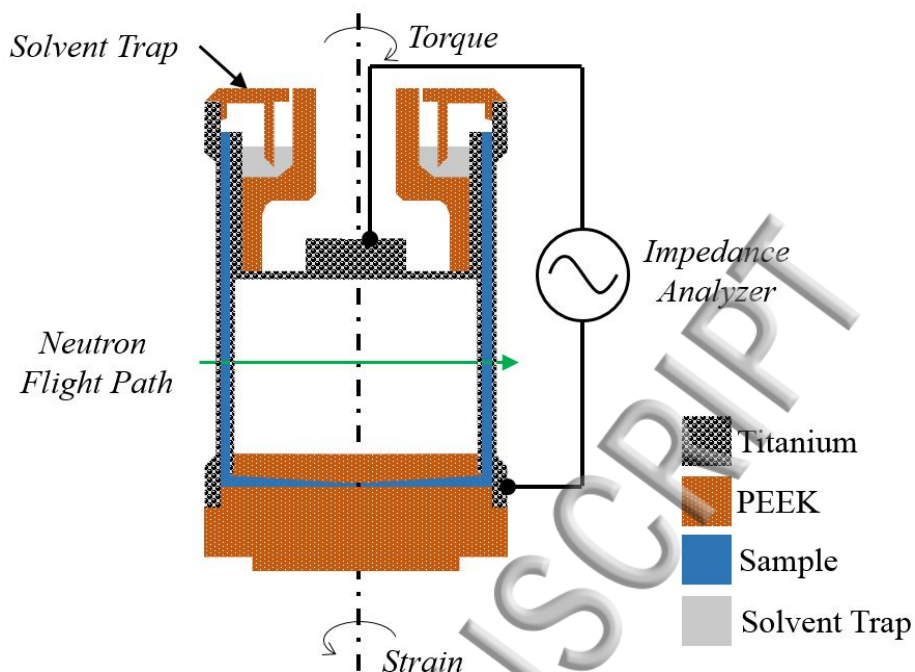


Figure 1: Cross-section of Dielectric RheoSANS geometry. Sample is contained in space between two cylinders.

Electrical contact with the bob wall is made at the center axis of the bob, while electrical contact with the cup wall is made at an exterior radial position on the bottom of the cup wall as shown in Figure 1. A silver paste bus bar ensures uniform distribution of current around the cup wall. In this rheometer, the cup rotates and the torque is measured by the bob. Therefore, in order to maintain electrical contact with the cup as it undergoes steady shear, a slip ring (Fabricast, Part#1972-2BR-FAG180) is mounted to the cup shaft, as described in a previous publication.²⁴ A composite carbon/silver brush mounted to the rheometer maintains electrical contact with the slip ring and provides for low noise and low frictional contact. A two-electrode measurement is made using an Agilent E4980 LCR meter with a 20 Hz to 2 MHz frequency range through electrical connections to the bob and the carbon brush.

III.B Modifications to Force Convection Oven

The entire Dielectric RheoSANS Geometry is contained within a Forced Convection Oven (FCO), an accessory that is commercially available with the ARES G2 rheometer. To facilitate SANS measurements, we modified the FCO to allow for the passage of incident and scattered neutrons over a wide angular range as highlighted in Figure 2. The instrument can be mounted on the NG-7 beam-line at the National Institute of Standards and Technology in Gaithersburg, Maryland and aligned to do SANS measurements over a wide Q-range (0.01 nm^{-1} to 2.5 nm^{-1}).²⁷ This provides microstructural information over an effective size range from 2 nm – 300 nm. To make the oven compatible with SANS measurements the stock ceramic inserts that control the convection within the oven were replaced with custom-made ceramic inserts that provide beam entry and exit pathways defined by the desired maximum beam size and scattering angle (17° at 0.6 nm wavelength neutrons) on the detector. This design enables access for probing both the radial (1,3) and tangential (2,3) shear planes of the Couette Geometry with SANS.²⁴ The modifications to the ceramic inserts are shown in Figure 2. These inserts were made by 3-D printing molds from ABS plastic with the desired oven geometry as the mold negative. A silica refractory compound was then casted in these molds (CER-CAST Fused Silica – Cotronics Corp, Brooklyn, NY). After the casting set, the entire mold was cured at 150°C . The ABS plastic was then dissolved in acetone, and the castings were fired at 400°C overnight to finish the curing process. Thin Mylar (0.001" thick) windows were mounted to the openings as transparent neutron windows. The ARES G2 FCO accessory has a reported temperature range from -90°C to 620°C when using the liquid nitrogen dewar. However, due to thermal expansion of the Dielectric RheoSANS Geometry, the use of Mylar windows, and the temperature limitations of the epoxy, the maximum accessible temperature range is limited to more restricted range of -50°C to 150°C .

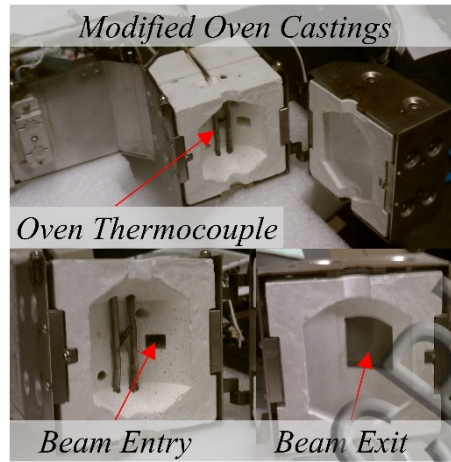


Figure 2. Diagram highlighting modifications to the FCO necessary to accommodate SANS experiments including the beam entry (15 mm wide and 10 mm tall) and exit ports (solid angle cut accommodating angular divergence of 17°).

III.C. Calibrations and Validation

III.C.1. Impedance Correction

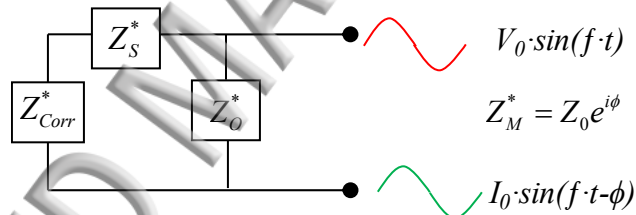


Figure 3. Schematic of the equivalent circuit diagram for the Dielectric RheoSANS measurement for the open and short circuit correction.

AC impedance measurements are made concentrically on the sample within the Couette.²⁸ The complex impedance, Z^* , is measured by applying a time-oscillating voltage characterized by a voltage amplitude, V_0 , and frequency, f . The measured linear response is then given by the current amplitude, I_0 , and the phase shift, ϕ . The resulting complex impedance of the system can then be calculated by $Z_M^* = I_0/V_0 e^{i\phi}$ where $i = \sqrt{-1}$. To quantify the electrical response of the sample, the instrument response must first be removed from the measured signal. The instrument

response (Figure 3) is modeled by two impedance elements; a resistor in series, Z_s^* , with the sample and a capacitor in parallel, Z_o^* , as shown in Figure 3.

$$\text{Equation 1.) } Z_{Corr}^* = \frac{(Z_M^* - Z_S^*)}{1 - (Z_M^* - Z_S^*)/Z_O^*}$$

By making a short circuit and open circuit measurement, Z_s^* and Z_o^* respectively, the system response, can be corrected, Z_{Corr}^* , per Equation 1. A typical open and short circuit measurement are shown in Figure 4a. Z' and Z'' are the real and imaginary components of the complex impedance, Z^* . The ideal dielectric response of the open and short circuit measurements is described by Equations 2 and 3 respectively.²⁹

$$\text{Equation 2.) } Z_o^* = -i/2\pi f C_o$$

$$\text{Equation 3.) } Z_s^* = R_s + i \cdot 2\pi f L_s$$

In these equations, R_s is the series resistance, L_s is the inductance of the short-circuited cell, and C_o is the capacitance of the empty cell. The geometry response shows very good agreement with Equations 2 and 3 at low frequencies. However, for frequencies exceeding ~10,000 Hz there is a frequency dependent component of the instrument response in the short-circuit measurement causing the resistance of the cell to increase with increasing frequency. This increase is a result of the electrode skin effect leading to non-uniform current distribution throughout the metallic conductors that comprise the cable connectors. The magnitude of the inductance imply that the short circuit response is not dominated by the sample geometry at high frequencies, but instead by the cable connections leading from the LCR meter to the geometry itself and therefore, should be independent of the resistivity of the material being tested.

Therefore, the frequency dependent short circuit response is directly subtracted to calculate Z_{Corr}^* .³⁰

A key design feature of the Dielectric RheoSANS instrument is that the instrument response is independent of the sample deformation and shear rate. This requires the cylinder eccentricity to

be maintained within a tight tolerance such that the parameters which describe the electrical response of the instrument do not vary with shear rate or strain. The alignment procedure for the Dielectric Couette is described elsewhere.²⁴ We have found that the alignment is adequate when the capacitance of the open cell varies by less than 0.5% under steady shear, a condition that can be reproducibly achieved using our design. When the geometry is well aligned, the relevant parameters describing the instrument response can be extracted by measuring a liquid metal (Gallium-indium eutectic – E-GaIn, Aldrich) under steady shear conditions at different rotation velocities, ω . The results interpreted using Equations 2 and 3 of the low-frequency impedance data are shown in Figure 4b to be independent of the shear rate. The cell constant and other dielectric parameters are summarized in Table 1.

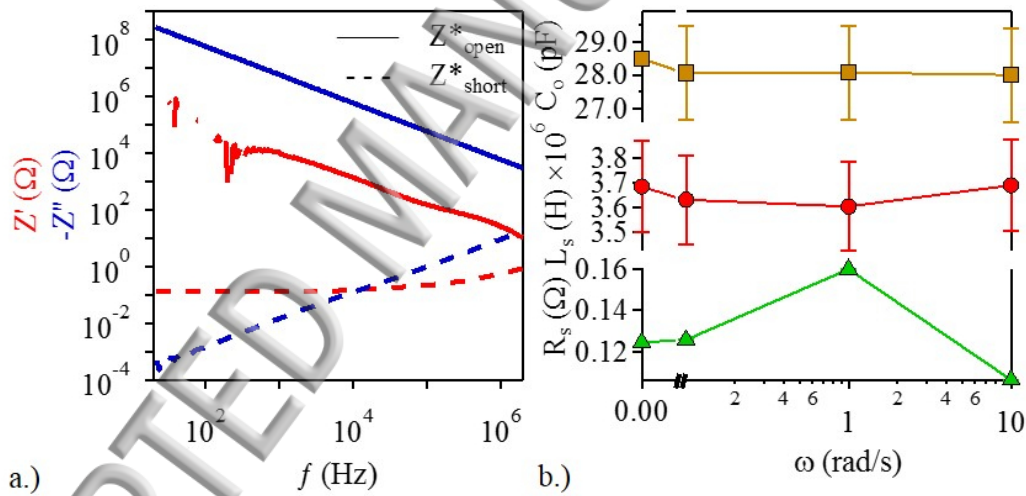


Figure 4. a.) Representative complex impedance versus frequency for open and short circuit measurements from the dielectric Couette geometry, b.) Open and short circuit parameters extracted from equivalent circuit modeling of the low-frequency conductivity data as a function of rotation rate, ω (rad/s). The short circuit measurements were made with E-GaIn filled within the Couette to facilitate measurements under steady shear. Error bars represent 1 standard deviation from the average.

III.C.2: Rheological Corrections

The conversion between shear stress, τ , and torque, M , are given in Equation 4.³¹

$$\text{Equation 4.) } \tau_{r,\theta} = K_M M \text{ where } K_M = \frac{(1+\delta^2)}{4\pi LR^2 \delta^2}$$

$$\dot{\gamma} = K_\omega \omega \text{ where } K_\omega = \frac{(1+\delta^2)}{(\delta^2 - 1)}$$

Here we assume that there are no end effects. In Equation 4, L is the length of the cup and R is the radius, δ is the ratio of the cup to bob diameter. The cone angle is machined such that the strain constant, K_ω , is closely matched to the Couette section 14.5 1/rad. A truncation gap of 100 μm is used for this geometry. Therefore, the theoretical stress constant, K_M , for the geometry is 25182 m^3 . Measurement of rheological standards show good agreement with the predictions from the geometry alone as shown in Figure 5. The normal force, F_z , from the sample confined underneath the cone can also be measured and converted to the normal stress coefficient, N_1 , using Equation 5.³¹ These calculations are summarized in Figure 5.

$$\text{Equation 5.) } N_1 = \tau_{11} - \tau_{22} = K_N F_z = \frac{2F_z}{\pi R^2}$$

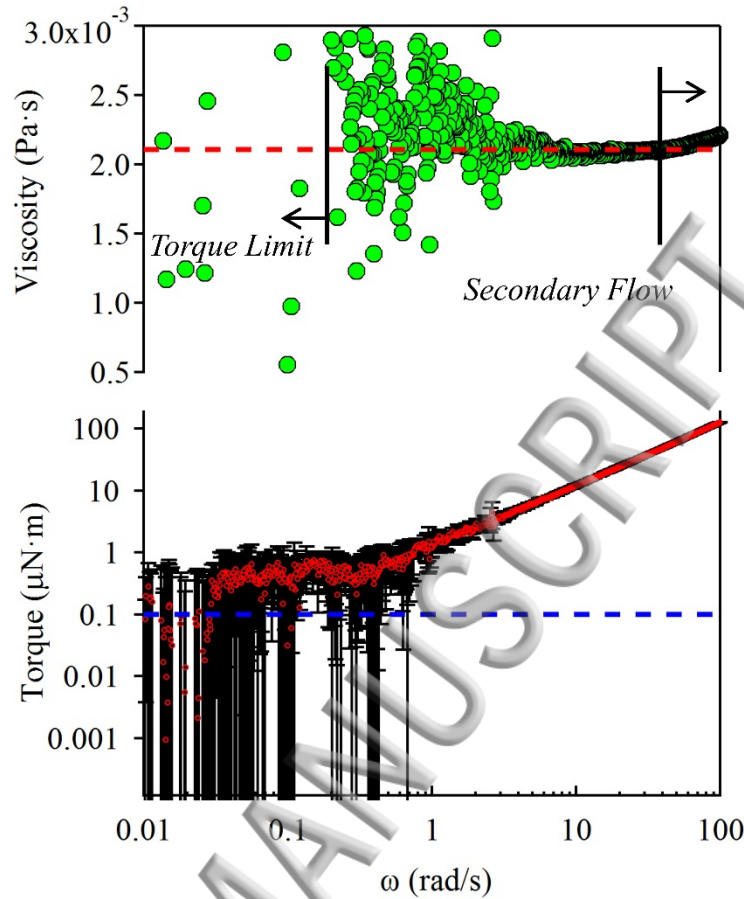


Figure 5. (top) Viscosity (Pa·s) and (bottom) Torque ($\mu\text{N}\cdot\text{m}$) versus rotational velocity, ω , (rad/s) for a Newtonian viscosity standard of 2.107 Pa·s measured at 25°C. Blue dashed line is torque limit of the rheometer. The red line marks the expected viscosity and solid black lines show the onset of secondary flows.

III.C.3: Scattering Corrections

Typical SANS configurations to cover the entire accessible Q-range employ 0.6 nm and 0.8 nm wavelength neutrons. Figure 6 summarizes the theoretical transmission of titanium as a function of titanium thickness and neutron wavelength. The transmission of the Dielectric Couette, T_{EC} , was determined to be 0.75 +/- .01 for $\lambda=0.6$ nm neutrons and 0.71 +/- .01 for $\lambda=0.8$ nm neutrons respectively. The empty cell scattering measurements show low coherent cross-section scattering as has been observed for other RheoSANS geometries machined from titanium with slight anisotropy at low-Q.³² The scattering from the Mylar windows is undetectable in our

measurements. The oven geometry attenuates the SANS signal at highest achievable Q-values as shown in Figure 6b. This region must be masked during the reduction process and limits the largest accessible Q-value to $Q < 2.5 \text{ nm}^{-1}$.

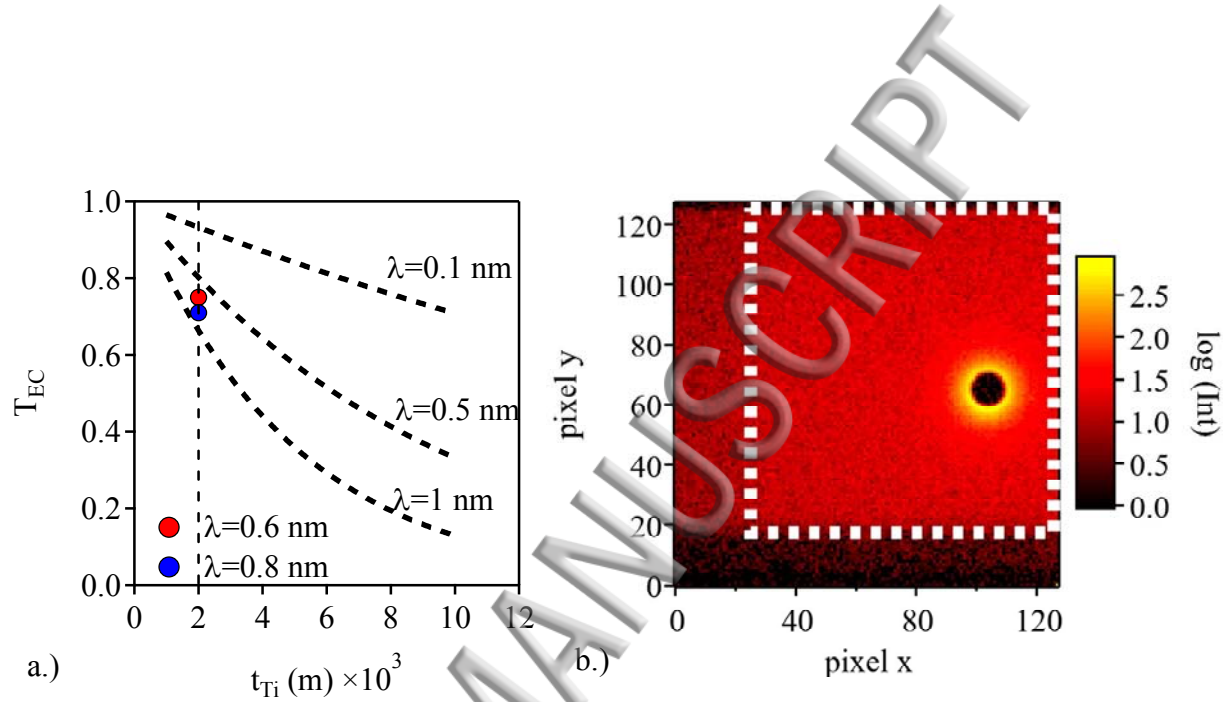


Figure 6. a.) Transmission calculation as a function of wavelength and thickness for titanium. Measured Quantities are shown for 2 mm thickness of the Dielectric Geometry, b.) Two-dimensional detector image of the 1m scattering data collected from Dielectric Couette within the FCO. The white box demarks the largest Q-range obtainable due to the occlusion of the oven geometry.

Table 1: Instrument Parameters for the Dielectric, Rheological and Scattering Measurements. All errors represent 1 standard deviation from the mean.

	Parameter	Value	Unit
Rheological	Stress Constant, K_M	25182 +/- 10	Pa/N·m
	Strain Constant, K_ω	14.5 +/- 1	1/rad
	Normal Stress Constant, K_N	4070 +/- 10	Pa/N
	Truncation Gap	100	μm
Dielectric	Conductivity Constant	2.94 +/- 0.06	1/m
	R_s	0.15 +/- 0.05	Ω
	C_o	28.4 +/- 0.2	pF

	L_s	1500 +/- 100	nH
SANS	T_{EC}	71 (0.8 nm), 75 (0.6	%
	Sample Volume	3.2-4.0	mL
	Maximum Beam Area	8	mm

III.D. SANS triggering and Clock Reset Protocol

A final critical component of the Dielectric RheoSANS experiment is the synchronization of the acquisition of the rheology, dielectric spectroscopy and small angle neutron scattering data during a test. This is enabled using event mode triggering protocol. In event mode processing, each neutron event that is detected on the two-dimensional SANS detector is recorded in a single line of binary containing the arrival time and x, y pixel position. Each list entry contains the pixel values defined as two 8-bit integers and the time value. To accommodate experimental times exceeding the allocated memory size for each entry, the detector clock is reset at a known periodic interval that corresponds to 2^{26} time intervals, which with 100 nanosecond resolution, corresponds to ~ 6.71 seconds. The first step in data processing for event mode data is to reconstruct the relative arrival time of neutrons during an experiment using this list. This is accomplished through the rolling addition of accumulated neutron time based on these clock resets. While this procedure can allow for reconstitution of time-dependent neutron scattering experiments, it is prone to errors associated with neutron event detection, corruption of data written to the buffer, and inaccurate interval times. While some of these errors are corrected automatically by the Igor Pro Event Mode Loader function provided by the IGOR Pro SANS reduction macros used by the NCNR, residual time errors can remain in the data sets.³³ These residual time errors are infrequent but can accumulate throughout the course of long acquisitions to 100's of seconds of absolute time error. Fortunately, time errors are easily identified as

discontinuities in the derivative, $\Delta t/\text{event}$, of the difference in neutron time per neutron event.

Events that are near a time-error will have large and sometimes negative $\Delta t/\text{event}$ corresponding to greater than 100 ms difference per event detected. Such values are physically impossible given the neutron flux (10^7 neutrons/cm²/s) and are a result of miscorrection of the total accumulated neutron time. By scrolling through the accumulated neutron time list, events that occur with $|\Delta t/\text{event}| > 100$ ms are assumed to be time correction error and a final correction is applied to the data. Using this protocol, absolute neutron time can be accurately reconstructed.²⁶

Synchronization of absolute neutron time with the rheological and dielectric data acquisition is achieved using an analogue triggering protocol that has been developed at the NCNR that permits a user-reset of the detector clock at time-intervals that do not correspond to the memory limited clock reset. This requires an analogue 5 V signal pulse with a specified peak width of at least 1 millisecond to be sent to the detector that resets on the trailing edge of the pulse. Using this protocol, manual trigger resets provide a means to synchronize the SANS acquisition with the motion of the rheometer with a temporal resolution of, in principle, 10's of milliseconds limited primarily by the finite flight time of the neutrons from the sample to the detector.²⁰

In a typical Dielectric RheoSANS experiment, these capabilities are harnessed. The detector is maintained at a fixed position and event mode data is continuously acquired as a preprogrammed set of experimental protocols are executed by the rheometer. The detector clock is reset at periodic intervals corresponding to the actions taken by the rheometer. In this way, when the rheometer commences a test or changes condition, the time of that change is encoded within the same SANS event mode file. Impedance measurements are similarly made as a function of frequency and time and are linked to the actions of the rheometer via a similar mechanism and stored in a separate text file. These actions are controlled by a Labview code and data acquisition

code that monitor the rheometer state, the elapsed experiment time, and coordinates the actions of the LCR meter. For a typical experiment protocol of a Dielectric RheoSANS experiments, the many processes that are overseen by the Labview code limit temporal resolution to ~ 200 ms. This is more than sufficient for steady shear experiments and allows for the reconstitution of the entire time-evolution of the dielectric, rheological and microstructural properties of a sample. After the test, the event mode data stream and the impedance data can be separated and then analyzed and corrected based on the experiment time and rheometer state. The raw SANS event mode data can be further reduced using standard reduction protocols by accounting for empty cell, dark current, and sample transmission and converted to absolute scale.³³

IV. Results:

The Dielectric RheoSANS instrument has been demonstrated on the NG-7 SANS beamline at the NIST Center for Neutron Research (NCNR) at the National Institute of Standards and Technology (NIST) in Gaithersburg, MD.³⁴ For all subsequent results, the sample aperture was rectangular with a 1×6 mm cross-section. To demonstrate the capability of the instrument, we have provided two examples where the simultaneous interrogation of the microstructure of a sample is coupled with its rheo-electric properties. As will be shown, our unique synchronization protocol and hardware provide high resolution kinetic and steady state information about materials as they undergo self-assembly and deform under applied shear flow.

IV.A Poly(3-hexylthiophene) Organogels:

Electrical conductivity in conjugated polymer based composites has gained increasing attention in recent years with the advent of efficient conjugated polymer based electronic devices. Of fundamental interest is the connection between the microstructure of the polymer phase and its electrical properties. Many conjugated polymers associate in solution to form semi-crystalline

phases with distinct electronic characteristics from their soluble counterparts, which has important implications both for thin-film processing and for fundamental understanding of charge transport in these materials. To study these relationships recent work has focused on the use of small angle scattering methods in combination with both conductivity measurements and rheology to identify microstructural characteristics such as branching that are consequential in achieving high conductivity materials. Regio-regular poly(3-hexylthiophene) (P3HT) is frequently used as a model system for this purpose owing to its propensity to form extended fibrillar structures with nanoscale cross-sections both in solution and in thin-films.³⁵ These structures facilitate long range charge transport via inter-chain exciton hopping within the fibrillar domains. Solutions consisting of P3HT dissolved in a moderate solvent have been observed to undergo a thermally reversible sol-gel transition where the gel consists of a network of interconnected fibers. Dielectric RheoSANS is an ideal technique to study the self-assembly of these fibers into gels as it combines both the electrical characterization and rheological characterization in the same measurement. In order to demonstrate the feasibility of doing detailed experiment on such samples, we have measured 20 mg/mL (P3HT) in a mixture of deuterated d_{34} -hexadecane/ d_4 -dichlorobenzene (30% weight fraction hexadecane) as described elsewhere.³⁶ Dichlorobenzene is a good solvent for P3HT and hexadecane is a non-solvent. They are chosen due to their low volatility and their ratio selected such that strong organogels form at room temperature.³⁷

The SANS measurement for the interrogation of the P3HT Organogel sample as it assembles in solution was performed at a single configuration – $\lambda=0.6$ nm with $\Delta\lambda/\lambda=14\%$ and a 13-m detector position covering the Q-range from $0.05 \text{ nm}^{-1} < Q < 0.4 \text{ nm}^{-1}$. At the beginning of this test, the temperature was stepped from 40°C to 25°C while both the complex impedance ($f=2$ kHz) and

The rheological response was monitored using a small amplitude oscillatory test ($f=1$ Hz and $\gamma_0=0.001$). The ac conductivity σ_{AC} (S/m), the elastic modulus, G' (Pa), and viscous modulus, G'' (Pa), were monitored as a function of time after the temperature quench. The corrected signal values are shown in Figure 7a. Additionally, event mode neutron acquisition was used to monitor the microstructural evolution of the sample during the test. The scattering events were accumulated into a histogram corresponding to the number of detector counts as a function of time. This is shown along with the electrical and mechanical response of the sample as it undergoes gelation in Figure 7a. While the count rate is uncorrected, it is related to the conversion of dissolved polymer chains into extended fibrillary structures. This is further confirmed by the $I(Q)$ dependence calculated by binning all the neutrons that arrive at the detector within a specified 100 second interval and reducing the resulting 1-D profiles to absolute scale using traditional correction methods as shown in Figure 7b.

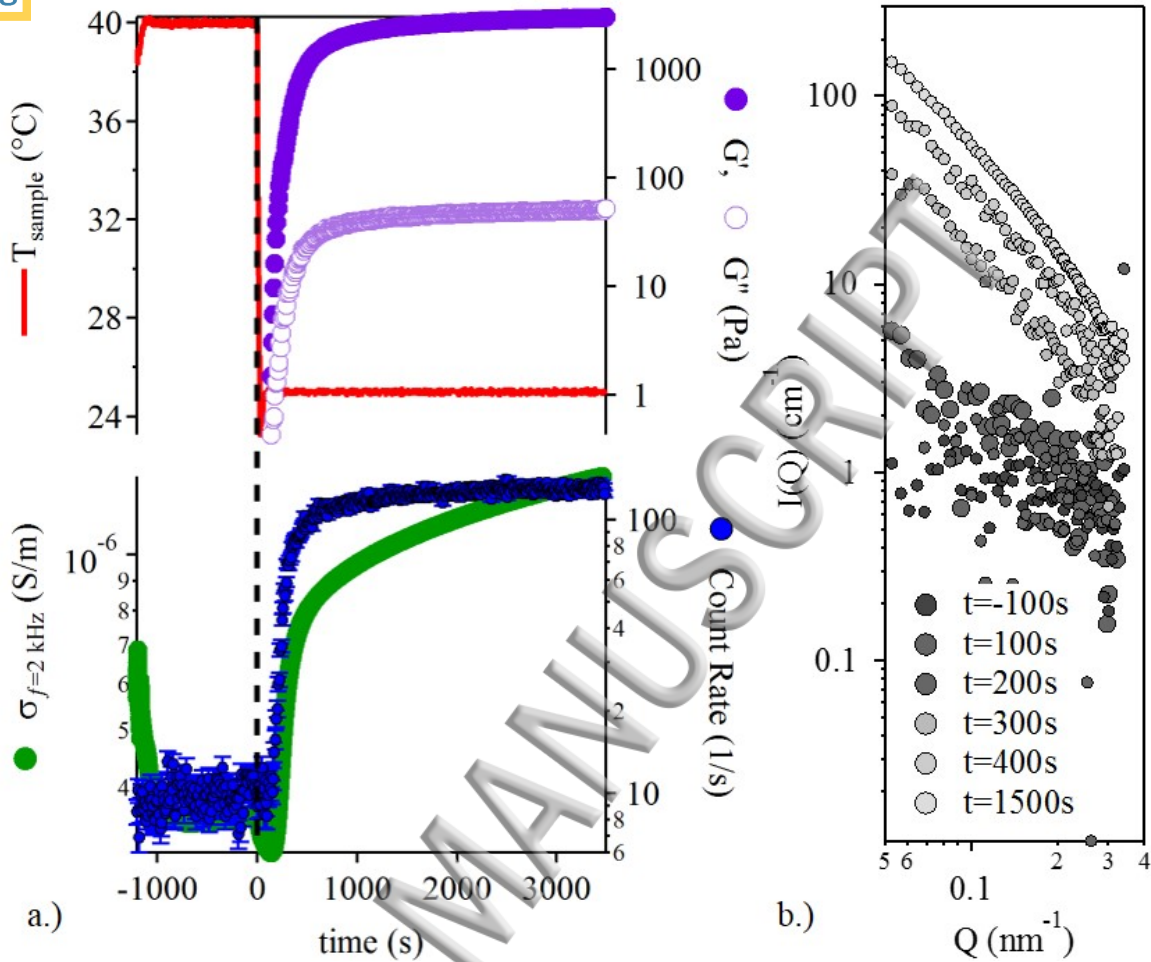


Figure 7: P3HT Dielectric RheoSANS Summary – a.) *top* – Elastic and Viscous Moduli ($f=1$ Hz and $\gamma_0=0.001$). Temperature as a function of experiment time, *bottom* – AC conductivity and Count Rate versus experiment time, b.) Reduced 1-D SANS, $I(Q)$ vs Q , profiles taken as a function of time corresponding to the time since quench in Figure 7a. Error bars represent 1 standard deviation from the average.

As is evident from Figure 7, the nucleation and growth of fibers is rapid, occurring within ~ 150 s of the beginning of the quench. Fiber formation is indicated by the increase in the scattering count rate, the increase in ac conductivity and the finite elastic modulus. Fiber formation continues to evolve and reaches ninety percent of its terminal value within 10 minutes of the quench. After an hour at 25°C the evolution of the conductivity and the elastic modulus also reaches within 90% of their steady state values. These results are consistent with previous

measurements of not only the electrical properties but also the viscoelastic and scattering measurements of P3HT organogels.³⁷

Further, as the count rate is proportional primarily to the volume fraction of nanofibers present in the solution, time-binning of the neutrons allows for direct comparison of the growth rate of fibers with the rheological and electrical properties with time bin as small as 10 seconds. This is in contrast to previous measurements that used one-minute time bins to determine the microstructural evolution of the samples.³⁶ Importantly, because all three measurements are made on the exact same sample at the exact same time, they are directly comparable. Figure 8a shows the conductivity, elastic modulus and count rate normalized per Equation 6 plotted versus $t-t_{\text{gel}}$, where t_{gel} is identified as the time G' and G'' cross-over.

$$\text{Equation 6.} \quad \Theta(t) = \frac{X(t) - X(0)}{X(\infty) - X(0)}$$

Because the data are taken simultaneously these reduced properties can be used to directly probe the effect of fiber growth on the gelation behavior with a 10 second resolution. This is shown in Figure 8b. Here, the reduced conductivity, Θ_{elect} , and reduced elastic modulus, Θ_{rheo} , are plotted against reduced count rate, Θ_{SANS} . Because Θ_{SANS} in this Q-range is proportional to the increase in volume fraction of fibers, Figure 8b effectively removes the time-dependent evolution of the material properties and instead relates both the elastic and electrical properties to the increasing volume fraction of fibers. In this representation, two growth regimes are clear. In the early stage of fiber growth, the elastic modulus and conductivity are strong functions of Θ_{SANS} . In the late stages of gelation, the elastic modulus exhibits a stronger power-law dependence with Θ_{SANS} suggesting a new growth mechanism. The fact that the conductivity is only weakly affected by

the process suggests that the transition from linear fiber growth to branching may be responsible for the different regimes. This is due to the contribution of branching to the mesh size of the network comprising the gel. While the elastic modulus is very sensitive to mesh size, increased branches results in more dead-ends and therefore has a weaker effect on the conductivity.

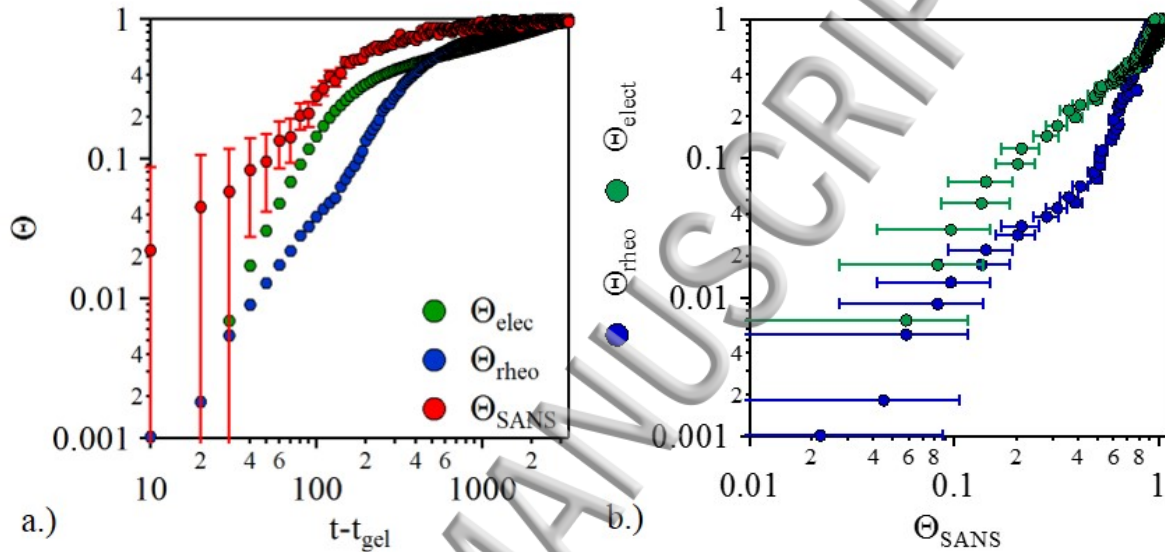


Figure 8. a.) Reduced electrical, rheological, and SANS properties plotted versus $t-t_{gel}$, and b.) the reduced conductivity, Θ_{elec} , and reduced elastic modulus, Θ_{rheo} , plotted against reduced count rate, Θ_{SANS} . Error bars are calculated as one standard deviation from the average on the count rate.

These results are consistent with previous observation of the intrinsic link between branching, connectivity and conductivity and for the first time are measured on the same sample as it assembles.^{22,38,39} The Dielectric RheoSANS instrument provides improved time resolution compared with previous techniques and the unique combination of all three measurements provides for quantitative comparison between the mechanisms underlying the conductivity and elasticity of these conjugated polymer organogels. Finally, Dielectric RheoSANS enables new protocols that are not currently possible with any other technique including monitoring rheo-electric response of P3HT fibers during gelation under applied shear, which has been suggested

to hinder branching and allow for the growth of longer fibers with intrinsically lower network connectivity.²²

IV.B Ionic Liquid Gels that Align under Steady Shear

Ion gels have recently found application in organic electronics owing to their high capacitance, excellent thermal and chemical stability, and ability to be processed using low-temperature casting methods. While the elastic properties of the gel network are a function primarily of their mesh density, the ionic conductivity is influenced by the relative free ion concentration and ion mobility. While a growing body of literature has investigated the effect of network architecture and polymer chemistry on the ion mobility in chemical cross-linked ion gels, physical gels formed via thermo-reversible self-assembly of Pluronic® micelles show promise as reconfigurable ion conductors. These physical ion gels form as a result of the self-assembly of block copolymers to form micelles that at a critical temperature and volume fraction form crystalline mesophases in ionic liquids.⁴⁰

A recent question regarding the development of these advanced ion gels is the role that the crystalline mesophase plays in determining ion mobility. It has been previously shown by Lopez-Barron et al. that crystalline mesophases can be reoriented and aligned in the shear direction producing high quality single crystalline phases.¹⁹ This system provides an excellent model to test the dependence of the ion conductivity as a function of crystalline order, a parameter that may inform the design of advanced thin-film structures. Dielectric RheoSANS is the ideal measurement to test this question as the AC conductivity can be monitored as the sample is subjected to increasing shear rate. This AC response can then be related to the intrinsic ion mobility and because the SANS data is acquired simultaneously, the degree of alignment and order of the crystallite can be compared with the evolution of conductivity. Therefore, as the

second case study to demonstrate the utility of Dielectric RheoSANS experiment, we performed a flow sweep test consisting of 13 shear rates where the shear rate was stepped from 0.001 1/s to 45 1/s logarithmically. The shear rate was held steady for 1800 seconds at each shear rate.

The SANS configuration for this study was $\lambda=0.6$ nm with $\Delta\lambda/\lambda=14\%$ and a 4-meter sample-to-detector distance covering the Q-range from $0.07 \text{ nm}^{-1} < Q < 0.8 \text{ nm}^{-1}$. At the beginning of the experiment, the temperature was ramped from 10 °C to 40°C and equilibrated. The static SANS pattern was then measured to confirm the formation of a gel consisting of an isotropic crystalline mesophase. The flow sweep was then initiated and the frequency dependent complex impedance and shear stress were recorded as a function of time and shear rate. Event mode neutron acquisition was used to monitor the microstructural evolution of the sample during the test and the detector clock reset between each shear rate to ensure synchronization over the course of the long acquisition. At the end of the test, scattering events corresponding to steady state in the shear stress (the last 300 seconds of each shear rate) were accumulated into a 2-D histogram $I(Q_x, Q_y)$ and reduced to absolute scale.

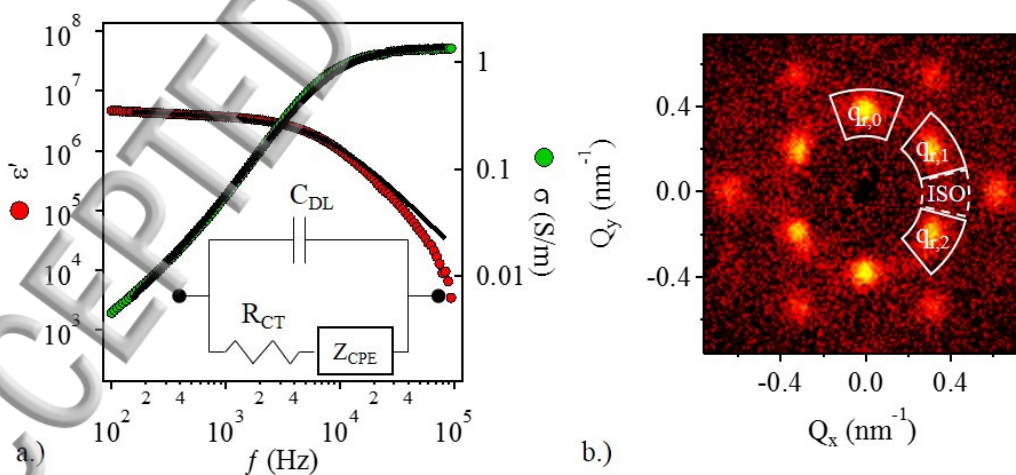


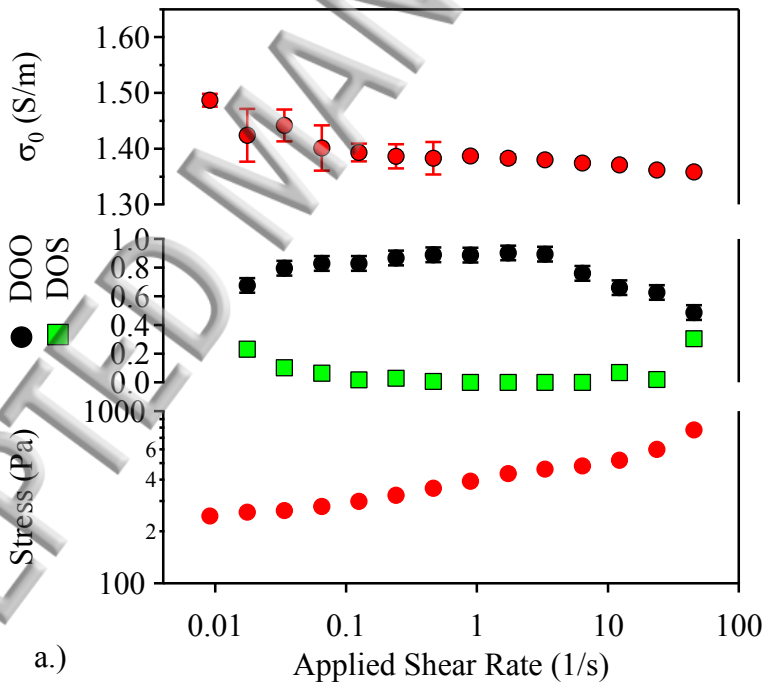
Figure 9. a.) Permittivity and conductivity (S/m) versus frequency (Hz) with Randle's Circuit model overlaid, and b.) Corrected 2-D SANS pattern plotted versus Q_x and Q_y . The regions in white are those that are integrated to calculate DOO and DOS.

A representative dielectric sweep consisting of the conductivity and the permittivity of an ion gel is plotted against the frequency is shown in Figure 9. The data is fit using complex non-linear least squares method to the equivalent circuit model of a Randle's Circuit with constant phase element that accounts for the polarization of the electrode.³⁰ This circuit describes the dielectric response from an ionic solution and the charge transfer resistance can be used to calculate the DC conductivity, $\sigma_0 = k/R_{CT}$, where k is the inverse of the conductivity constant. This fitting protocol is applied for the impedance measurements made during the last 300 seconds of each shear rate where the shear stress was at steady state. The results of the analyzed data are shown in Figure 10a.

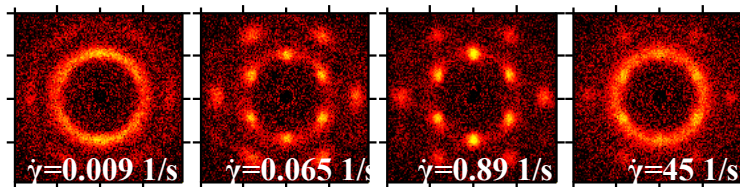
In order to characterize microstructural changes related to the alignment of the crystallites under steady shear, the reduced 2-D detector images are analyzed according to previously developed protocols.³³ Briefly, we take sector integration of the intensity in regions shown in Figure 9b along the $d_{r=\langle 110 \rangle}$ projection of FCC lattice which corresponds to the primary reflection of a hexagonal lattice. As the crystalline mesophases align the isotropic powder ring sharpens giving rise to $q_{r,0}$, $q_{r,1}$, $q_{r,2}$ reflections becoming more pronounced over the isotropic background. To quantify relative changes in alignment of the crystal, the degree of order (DOO) and degree of slipping (DOS) are calculated per the following equations $DOO = (I_{r,1} - I_{iso})/I_{r,1}$ and $DOS = 1 - (I_{r,0} - I_{iso})/(I_{r,1} - I_{iso})$. This procedure is performed at every shear for the steady state SANS data.

The results of the dielectric and SANS analyses of the ion gel are plotted in Figure 10 along with the shear stress as it undergoes the flow sweep experiment. As can be seen from the figure as the shear rate increases there is weak decrease in the dc conductivity but a dramatic change in the ordering of the crystalline mesophase as indicated by the increase in the DOO approaching

ing). At shear rates in excess of 3 1/s shear induced melting occurs leading to a reduction in order. This is further demonstrated by the 2-D detector images in Figure 10b. Coincident with these observations is that as the DOO increases, the DOS decreases. This has been previously ascribed to twinning.⁴¹ These results agree well with previously published results and the shear stress extracted from the steady state rheology of the sample. The Dielectric RheoSANS experiment points to the fact that microstructure for this sample plays a negligible role in determining the ion mobility. Despite the dramatic microstructural rearrangements, only slight changes in conductivity are observed further confirming the fact that the ionic liquid is only modestly confined within the crystalline domains. Therefore, alignment does not significantly change its confinement.



a.)



b.)

Figure 10. a.) Steady state electrical – conductivity (S/m), microstructural –DOO and DOS, and rheological – shear stress plotted versus applied shear rate (1/s), b.) Representative steady state 2-D detector images selected to demonstrate the evolution of mesophase alignment under applied shear. Error bars represent 1 standard deviation from the average.

V. Conclusions.

In this work, we have detailed the development and validation of a new Dielectric RheoSANS instrument and demonstrated its application in two test cases. We have demonstrated how both steady shear and kinetic studies can be performed simultaneously measuring electrical rheological, and microstructural properties. Importantly, these measurements are all made on the same region of interest within the sample such that the results can be directly and unambiguously compared. This opens new opportunities to study materials using complex experimental protocols, as well as thixotropic materials with complicated sample histories. The case studies presented here show that the instrument can track with excellent time resolution the structural origins of the gelation of the conjugated polymer P3HT and demonstrate that the shear induced structural changes do not significantly affect the electrical response of an ionic liquid gel phase. These examples demonstrate the utility of the Dielectric RheoSANS instrument for examining the microstructural origins of the rheo-electric properties of soft matter materials. Further the instrument provides a flexible platform for the interrogation of a wide range of potential experimental protocols as a generic RheoSANS instrument with expanded temperature capability. The instrument is available for use at the NIST Center for Neutron Research.

VI. Acknowledgements.

The authors would like to acknowledge funding from the NIST Center for Neutron Research cooperative agreements #70NANB12H239 & 70NANB15H260, the NCNR CMS grant for partial funding during this time as well as the National Research Council for support. This work

benefitted from SasView software, originally developed by the DANSE project under NSF award DMR-0520547. We would also like to thank Greg Newbloom and Ru Chen for providing useful discussions and samples for the case studies in this manuscript. Finally, Cedric Gagnon and Jeff Krzywon for their assistance in preparing the sample environment. Certain commercial equipment, instruments, or materials are identified in this paper to specify the experimental procedure adequately. Such identification is not intended to imply recommendation or endorsement by the National Institute of Standards and Technology, nor is it intended to imply that the materials or equipment identified are necessarily the best available for the purpose.

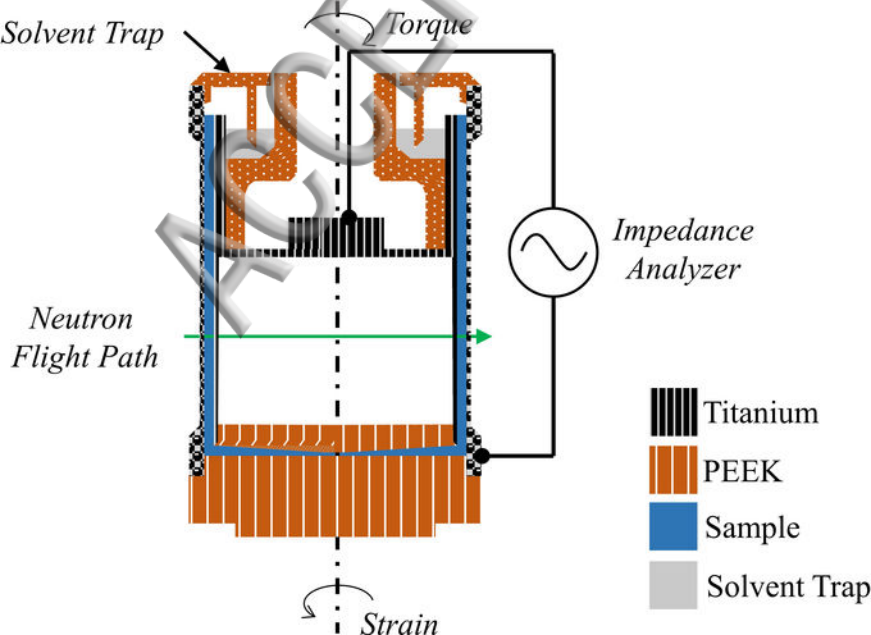
REFERENCES.

- 1 A. Narayanan, F. Mugele, and M.H.G. Duits, *Langmuir* **33**, 1629 (2017).
- 2 A. Helal, T. Divoux, and G.H. McKinley, *Phys. Rev. Appl.* **6**, 64004 (2016).
- 3 J. Mewis, L.M. de Groot, and J.A. Helsen, *Colloids Surf.* **22**, 271 (1987).
- 4 B.P. Sahoo, K. Naskar, and D.K. Tripathy, *J. Elastomers Plast.* **46**, 675 (2014).
- 5 K. Miyasaka, K. Watanabe, E. Jojima, H. Aida, M. Sumita, and K. Ishikawa, *J. Mater. Sci.* **17**, 1610 (1982).
- 6 Y. Matsumiya, K. Kumazawa, M. Nagao, O. Urakawa, and H. Watanabe, *Macromolecules* **46**, 6067 (2013).
- 7 H. Watanabe, Y. Matsumiya, and T. Inoue, *Macromolecules* **35**, 2339 (2002).
- 8 M.E. Helgeson, P.A. Vasquez, E.W. Kaler, and N.J. Wagner, *J. Rheol.* **53**, 727 (2009).
- 9 A.K. Gurnon, P.D. Godfrin, N.J. Wagner, A.P.R. Eberle, P. Butler, and L. Porcar, *J. Vis. Exp.* **84**, e51068 (2014).
- 10 N.J. Wagner, *Curr. Opin. Colloid Interface Sci.* **3**, 391 (1998).
- 11 N.J. Wagner and J.F. Brady, *Phys. Today* **62**, 27 (2009).
- 12 J. Stellbrink, B. Lonetti, G. Rother, L. Willner, and D. Richter, *J. Phys.: Condens. Matter* **20**, 404206 (2008).
- 13 P.G. Cummins, E. Staples, B. Millen, and J. Penfold, *Meas. Sci. Technol.* **1**, 179 (1990).
- 14 G.C. Straty, H.J.M. Hanley, and C.J. Glinka, *J. Stat. Phys.* **62**, 1015 (1991).

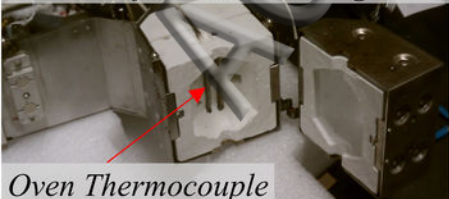
- 15 M.W. Liberatore, F. Nettesheim, N.J. Wagner, and L. Porcar, Phys. Rev. E - Stat. Nonlinear, Soft Matter Phys. **73**, 20504 (2006).
- 16 A.K. Gurnon, P.D. Godfrin, N.J. Wagner, A.P.R. Eberle, P. Butler, and L. Porcar, J. Vis. Exp. e51068 (2014).
- 17 A.P.R. Eberle and L. Porcar, Curr. Opin. Colloid Interface Sci. **17**, 33 (2012).
- 18 L. Porcar, D. Pozzo, G. Langenbacher, J. Moyer, and P.D. Butler, Rev. Sci. Instrum. **82**, 83902 (2011).
- 19 C.R. López-Barrón, N.J. Wagner, and L. Porcar, J. Rheol. **59**, 793 (2015).
- 20 M.A. Calabrese, N.J. Wagner, and S.A. Rogers, Soft Matter **12**, 2301 (2016).
- 21 A.P. Kotula, M.W. Meyer, F. De Vito, J. Plog, A.R. Hight Walker, and K.B. Migler, Rev. Sci. Instrum. **87**, 105105 (2016).
- 22 J.J. Wie, N.A. Nguyen, C.D. Cwalina, J. Liu, D.C. Martin, and M.E. Mackay, Macromolecules **47**, 3343 (2014).
- 23 G.M. Newbloom, K.M. Weigandt, and D.C. Pozzo, Soft Matter **8**, 8854 (2012).
- 24 J.J. Richards, C.V.L. Gagnon, J.R. Krzywon, N.J. Wagner, and P.D. Butler, J. Vis. Exp. e55318 (2017).
- 25 U. Genz, J.A. Helsen, and J. Mewis, J. Colloid Interface Sci. **165**, 212 (1994).
- 26 S.R. Kline and R.M. Dimeo, *2016 NIST Center for Neutron Research Accomplishments and Opportunities* (Gaithersburg, MD, 2016).
- 27 C.J. Glinka, J.G. Barker, B. Hammouda, S. Krueger, J.J. Moyer, and W.J. Orts, J. Appl. Crystallogr. **31**, 430 (1998).
- 28 C. Chassagne, D. Bedeaux, J.P.M.V.D. Ploeg, and G.J.M. Koper, Phys. A Stat. Mech. Its Appl. **326**, 129 (2003).
- 29 A.D. Hollingsworth and D.A. Saville, J. Colloid Interface Sci. **257**, 65 (2003).
- 30 E. Barsoukov and J.R. Macdonald, *Impedance Spectroscopy Theory, Experiment, and Applications* (2005).
- 31 C. Macosko, *Rheology: Principles, Measurements and Applications* (1996).
- 32 H.J. Wilson, J. Fluid Mech. **534**, 97 (2005).
- 33 S.R. Kline, J. Appl. Crystallogr. **39**, 895 (2006).
- 34 C.J. Glinka, J.G. Barker, B. Hammouda, and S. Krueger, J. Appl. Crystallogr. **31**, 430 (1998).
- 35 T. Salim, S. Sun, L.H. Wong, L. Xi, Y.L. Foo, and Y.M. Lam, J. Phys. Chem. C **114**, 9459 (2010).

- 36 G.M. Newbloom, K.M. Weigandt, and D.C. Pozzo, *Macromolecules* **45**, 3452 (2012).
- 37 G.M. Newbloom, P. de la Iglesia, and L.D. Pozzo, *Soft Matter* **10**, 8945 (2014).
- 38 G.M. Newbloom, F.S. Kim, S.A. Jenekhe, and D.C. Pozzo, *Macromolecules* **44**, 3801 (2011).
- 39 J. Liu, M. Arif, J. Zou, S.I. Khondaker, and L. Zhai, *Macromolecules* **42**, 9390 (2009).
- 40 C.R. López-Barrón, R. Chen, N.J. Wagner, and P.J. Beltramo, *Macromolecules* **49**, 5179 (2016).
- 41 C.R. López-Barrón, N.J. Wagner, and L. Porcar, *J. Rheol.* **59**, 793 (2015).

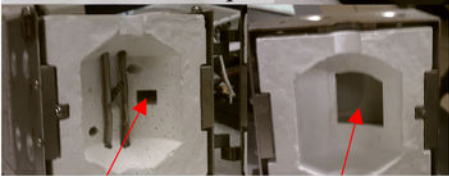
ACCEPTED MANUSCRIPT



Modified Oven Castings

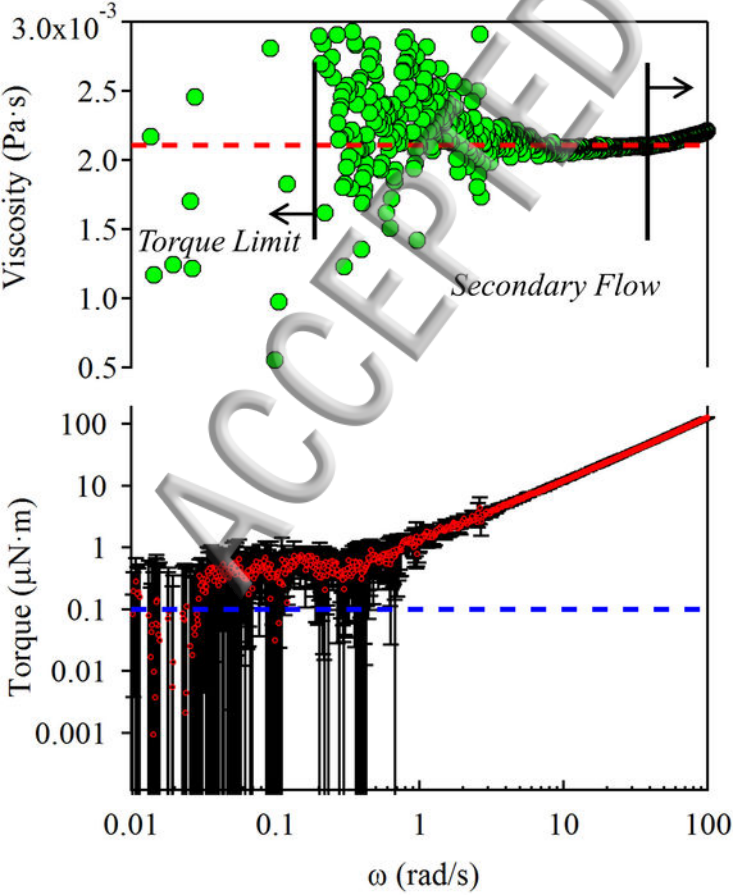


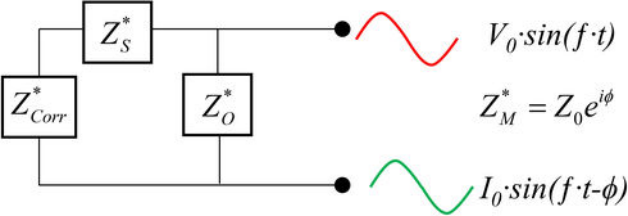
Oven Thermocouple

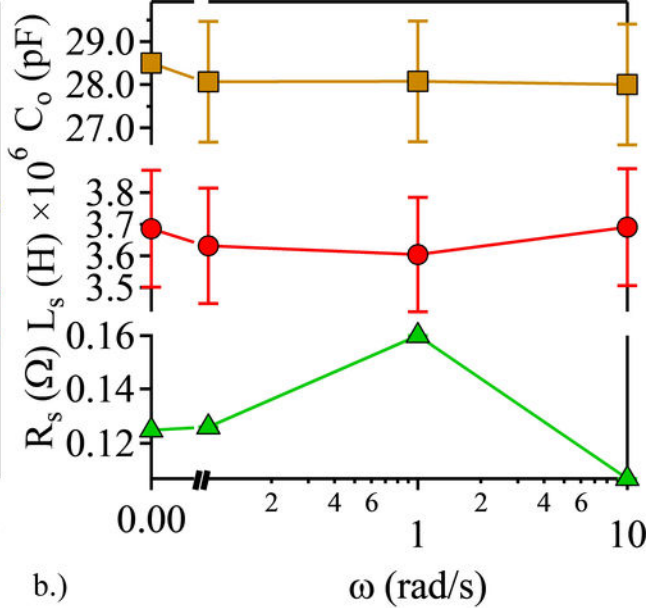
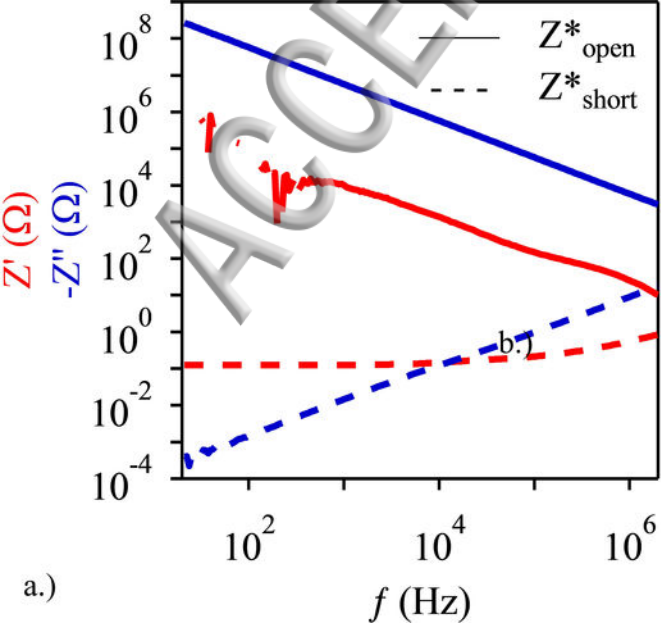


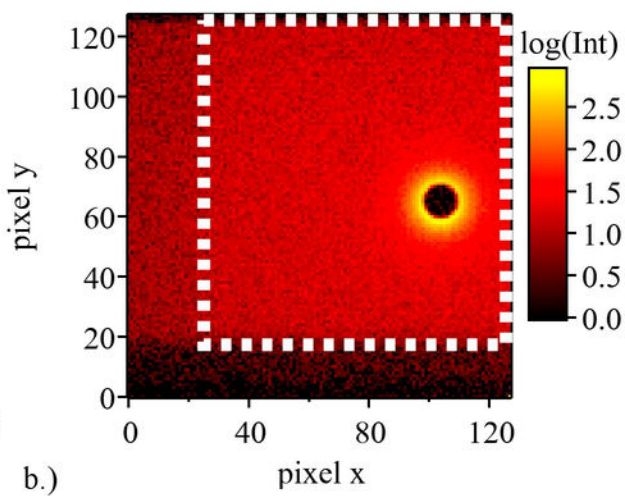
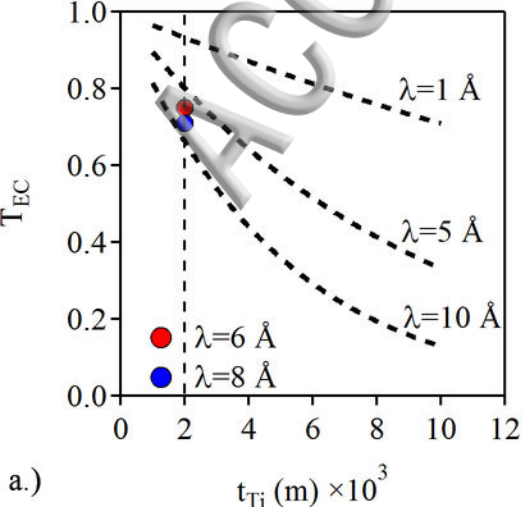
Beam Entry

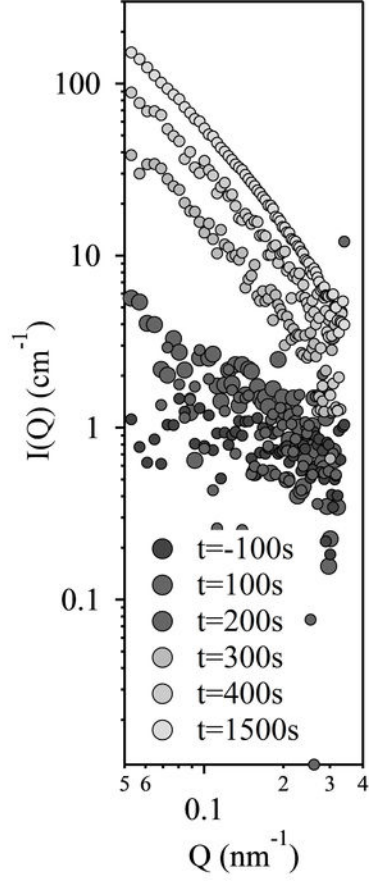
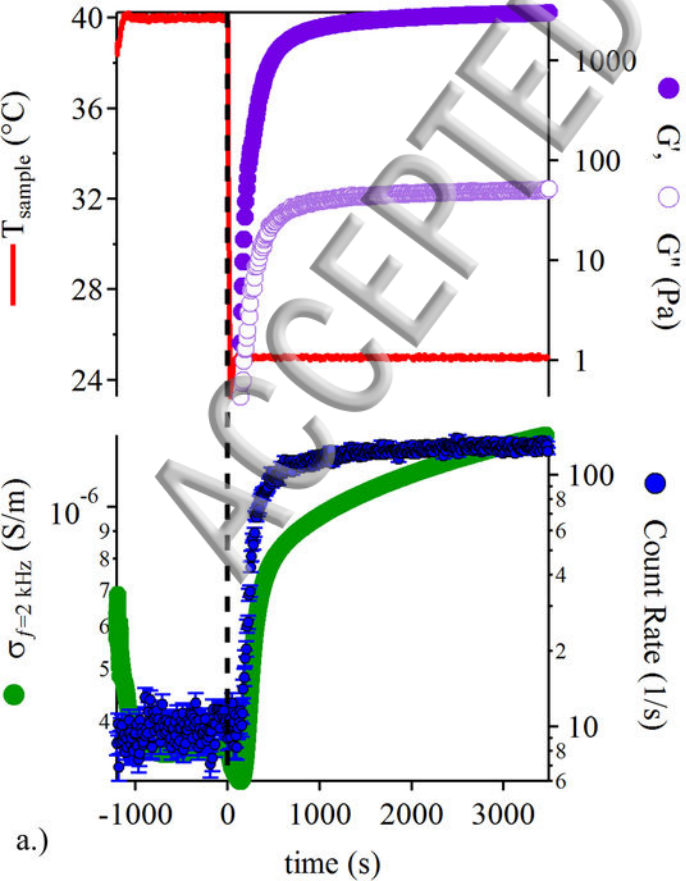
Beam Exit

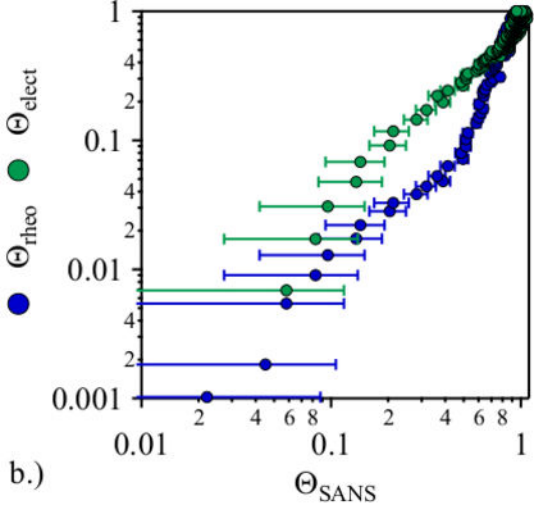
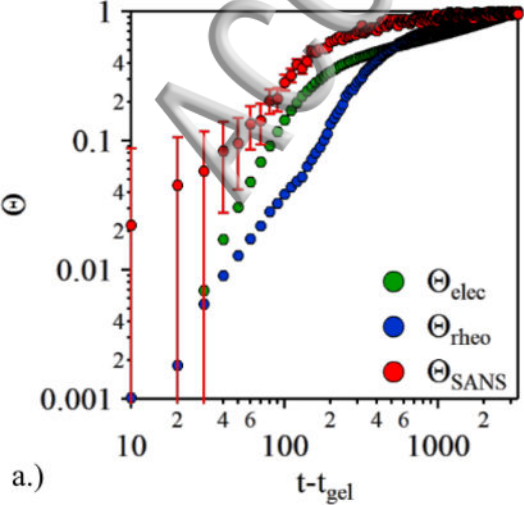


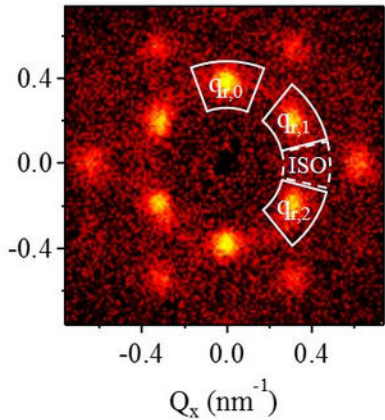
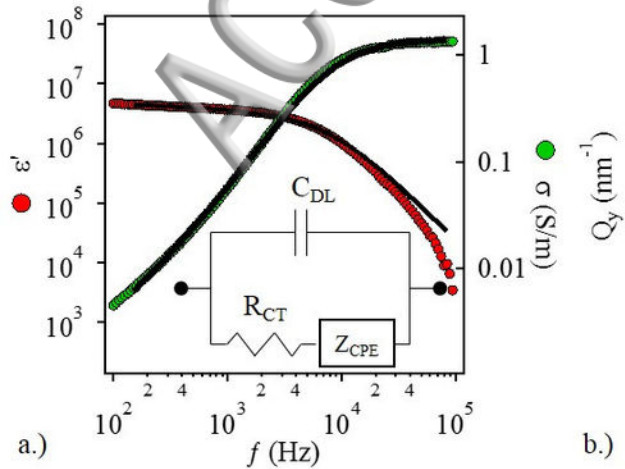


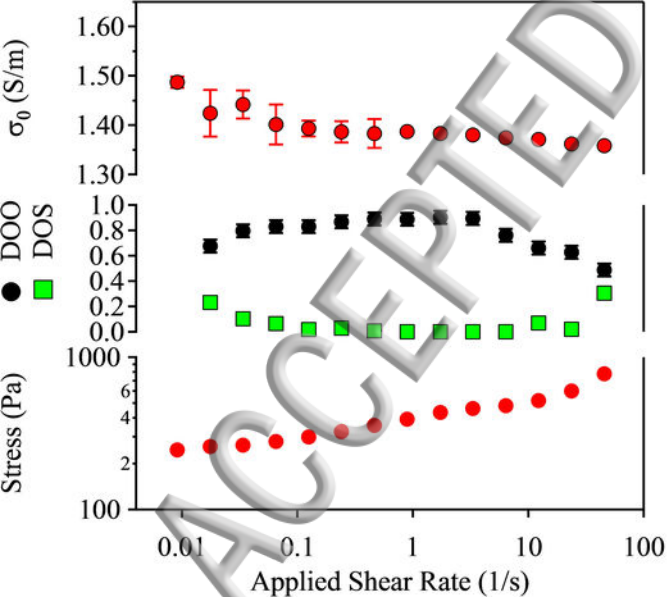




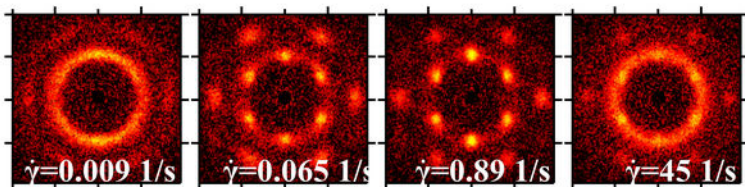








a.)



b.)